Frontiers of Information Technology & Electronic Engineering
www.jzus.zju.edu.cn; engineering.cae.cn; www.springerlink.com
ISSN 2095-9184 (print); ISSN 2095-9230 (online)
E-mail: jzus@zju.edu.cn

A general altitude-dependent path loss model for UAV-to-ground millimeter-wave communications*

Qiuming ZHU‡[1,2], Mengtian YAO[1], Fei BAI[1], Xiaomin CHEN‡[1],
Weizhi ZHONG[3], Boyu HUA[1], Xijuan YE[1]

[1]*The Key Laboratory of Dynamic Cognitive System of Electromagnetic Spectrum Space, College of Electronic and Information Engineering, Nanjing University of Aeronautics and Astronautics, Nanjing 211106, China*

[2]*State Key Laboratory of Integrated Services Networks, Xidian University, Xi'an 710000, China*

[3]*The Key Laboratory of Dynamic Cognitive System of Electromagnetic Spectrum Space, College of Astronautics, Nanjing University of Aeronautics and Astronautics, Nanjing 211106, China*

E-mail: zhuqiuming@nuaa.edu.cn; yaomengtian@nuaa.edu.cn; baifei@nuaa.edu.cn; chenxm402@nuaa.edu.cn; zhongwz@nuaa.edu.cn; byhua@nuaa.edu.cn; yexijuan@nuaa.edu.cn

Received Sept. 25, 2020; Revision accepted Feb. 20, 2021; Crosschecked May 11, 2021

Abstract: A general empirical path loss (PL) model for air-to-ground (A2G) millimeter-wave (mmWave) channels is proposed in this paper. Different from existing PL models, the new model takes the height factor of unmanned aerial vehicles (UAVs) into account, and divides the propagation conditions into three cases (i.e., line-of-sight, reflection, and diffraction). A map-based deterministic PL prediction algorithm based on the ray-tracing (RT) technique is developed, and is used to generate numerous PL data for different cases. By fitting and analyzing the PL data under different scenarios and UAV heights, altitude-dependent model parameters are provided. Simulation results show that the proposed model can be effectively used to predict PL values for both low- and high-altitude cases. The prediction results of the proposed model better match the RT-based calculation results than those of the Third Generation Partnership Project (3GPP) model and the close-in model. The standard deviation of the PL is also much smaller. Moreover, the new model is flexible and can be extended to other A2G scenarios (not included in this paper) by adjusting the parameters according to the simulation or measurement data.

Key words: Path loss; UAV-to-ground channel; Millimeter-wave (mmWave) communication channel; Ray-tracing; Altitude-dependent
https://doi.org/10.1631/FITEE.2000497 **CLC number:** TN928

1 Introduction

Unmanned aerial vehicles (UAVs) have shown great promise due to their high mobility and deployment flexibility (Chen et al., 2018; Zhu et al., 2018, 2019; Cui et al., 2019; Wang XY and Gursoy, 2019). Operating as airborne base stations (BSs) or flying relays, UAV-aided communication has attracted great interest in the fifth-generation and beyond fifth-generation (5G/B5G) mobile communications (Li et al., 2013; Wang CX et al., 2018; Zhang

‡ Corresponding authors

* Project supported by the National Key Scientific Instrument and Equipment Development Project, China (No. 61827801), the Aeronautical Science Foundation of China (No. 201901052001), the Fundamental Research Funds for the Central Universities, China (Nos. NS2020026 and NS2020063), the State Key Laboratory of Integrated Services Network Funding, China (No. ISN22-11), and the Open Foundation for Graduate Innovation of Nanjing University of Aeronautics and Astronautics (NUAA), China (No. KFJJ20200416)

ORCID: Qiuming ZHU, https://orcid.org/0000-0002-4995-5970; Xiaomin CHEN, https://orcid.org/0000-0002-9052-665X

et al., 2018; Dutta et al., 2019; Zhong et al., 2019a, 2019b; Cheng et al., 2020; Zhao et al., 2020; Zhu et al., 2020; You et al., 2021). The millimeter-wave (mmWave) technology is also a key component in the 5G/B5G system; more spectra can be used to provide greater data traffic (Fan et al., 2016; Hur et al., 2016). The path loss (PL) model can provide a theoretical basis for the system design and optimization of UAV-aided communications (MacCartney et al., 2015; Samimi et al., 2015; Sun et al., 2016; Rappaport et al., 2017a, 2017b; Khawaja et al., 2019; Yang et al., 2019). A thorough understanding of PL models and characteristics is essential for the system design and optimization of UAV-aided 5G/B5G communications.

In the literature, there are several widespread mmWave PL models, e.g., the close-in free-space reference distance (CI) model, the floating intercept (FI) model (or the ABG model), and the dual slope (DS) model (Rappaport et al., 2015). Both CI and FI models are based on a single slope model with the assumption that the characteristics do not change drastically, while the DS model has different slopes in different distance ranges. However, these models are based on transitional land mobile communication, where the maximum antenna height is limited.

Several empirical PL models for air-to-ground (A2G) scenarios have been addressed in Al-Hourani and Gomez (2018), Shi et al. (2018), Cai et al. (2019), and Cui et al. (2019). Al-Hourani and Gomez (2018) presented an A2G PL model based on extensive simulation data in a typical suburban environment. Cai et al. (2019) conducted channel measurements for characterizing the low-altitude A2G PL. Some UAV channel measurements at 1 and 4 GHz were provided in Cui et al. (2019), and a modified Third Generation Partnership Project (3GPP) PL model including line-of-sight (LoS) and non-line-of-sight (NLoS) cases was proposed. Shi et al. (2018) developed a log-distance PL model in the LoS and NLoS scenarios at 900 MHz, 1800 MHz, and 5 GHz. However, all of the above papers studied only the sub-6-GHz band channel. Due to device complexity and high cost, there are few A2G mmWave measurements.

The ray-tracing (RT) method is a deterministic way to model mmWave channels (Bhuvaneshwari et al., 2015; Wu et al., 2015; Mani et al., 2018). For example, Wu et al. (2015) developed a three-dimensional (3D) RT-based UAV-aided A2G channel model. In Bhuvaneshwari et al. (2015), by including diffraction effects in the RT method, a generalized channel model was proposed for the NLoS corridor scenario. In Mani et al. (2018), a PL model was investigated at 26 GHz in an urban scenario by combining measurements and RT simulations. However, these RT-based deterministic models require detailed descriptions of scenarios, scattering material characteristics, and transceiver's positions and orientations. Such information is often difficult to obtain, let alone the information on mobile scatterers such as vehicles, which are hard to quantitatively describe. Yang et al. (2019) proposed a stochastic A2G mmWave PL prediction method that applies the machine learning method on RT simulation data measured at 28 and 73 GHz; however, the details and the effect of UAV height were missing. This paper intends to fill in these research gaps. The main contributions and innovations are listed as follows:

1. A general parametric PL model for A2G mmWave channels is proposed. The new model considers not only the effects of scenario, distance, and frequency, but also the height factor, making it more suitable for A2G scenarios. Moreover, different from existing PL models that include LoS and NLoS cases, the new model consists of three cases, i.e., LoS, reflection, and diffraction, which can greatly improve the prediction accuracy.

2. A deterministic PL prediction algorithm based on the digital map and RT technique is developed. A detailed 3D scattering scenario reconstruction process is presented that can reduce the prediction complexity significantly.

3. To obtain proper parameters for the proposed PL model, numerous simulations are conducted by applying the map-based method to different specific scenarios with different UAV heights. By fitting the simulation data, the optimized model parameters are given and analyzed.

2 A2G mmWave propagation scenarios

A typical UAV-aided A2G communication link is shown in Fig. 1, and the terrestrial obstacles, e.g., buildings, trees, and vehicles, are referred to as scatterers.

For different scattering environments, the terrain is usually classified into four categories, i.e., flat, hilly, mountainous, and over water. The same

terrain can have a different cover, e.g., grass, forest, or buildings. For example, the recommended terrain covers in ITU (2017) include the rural open, tree-covered, built-up area, dry ground, wet terrain (no trees), fresh water, sea water, and so on. In this study, we merge some of these terrain covers because our previous work has revealed that they have similar effects on the PL of A2G mmWave channels.

The A2G scattering environments of this study are totally divided into 10 types (Fig. 2), including four terrains, each with different covers. Building is one of the main terrain cover types of flat terrain. According to the distribution of building size, height, and area density, flat terrain can be divided into suburban, urban, dense urban, and high-rise urban. Suburban and urban usually have sparse buildings and the building height is lower, but warehouses and other structures also affect channel characteristics. Hilly terrain is characterized by uneven ground height and occasional building cover. The channel

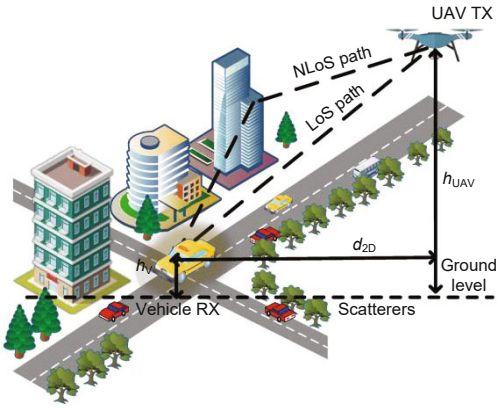

Fig. 1 A typical unmanned aerial vehicle (UAV) aided air-to-ground (A2G) mmWave communication link

h_{UAV}: height of the UAV antenna; h_V: height of the vehicle antenna; d_{2D}: horizontal distance between the UAV and the vehicle. TX: transmitter; RX: receiver

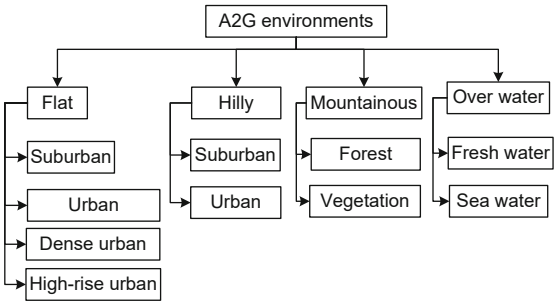

Fig. 2 Typical air-to-ground (A2G) mmWave communication environments

characteristics of mountainous terrain (which is divided into forest and vegetation) are greatly affected by the type and density of trees. The A2G propagation channel on the water surface is similar to that in an open environment. Compared with the ground, it has different surface reflectivity and roughness, and is divided into fresh water and sea water according to the difference in reflectivity.

3 Map-based deterministic path loss prediction

3.1 Flowchart of path loss prediction

The map-based PL prediction method aims to calculate the PL by using the RT technique on detailed information on the transceiver's location and scattering environment. The RT technique is based on the geometrical theorem of diffraction, uniform theory of diffraction (UTD), and field intensity superposition principle. Because the RT technique is very time-consuming depending on the scene complexity, it is necessary to simplify the digital map with an acceptable precision error. In this study, the proposed PL algorithm includes mainly two steps, i.e., reconstruction of the scattering scenario and PL calculation (Fig. 3). Based on the reconstructed 3D digital map, the RT technique is applied to track all possible propagation rays, i.e., direction, reflection, and diffraction, and then the PL value is obtained.

3.2 Three-dimensional scattering scenario reconstruction

Applying the RT technique requires detailed geometric and electromagnetic descriptions as input, which reflects the scattering environments and should be stored in the database in an appropriate format. The computation time largely depends on the database size. The reconstruction is of great significance in reducing the size of the database but ensures the prediction accuracy.

In this study, we reconstruct the scattering database with terrain and building information in two steps. First, the original map in the form of a digital elevation model (DEM) can be downloaded from Google Maps; it contains detailed information about latitude, longitude, and elevation of all points. The information would be used to reconstruct many triangle facets to roughly describe the terrain

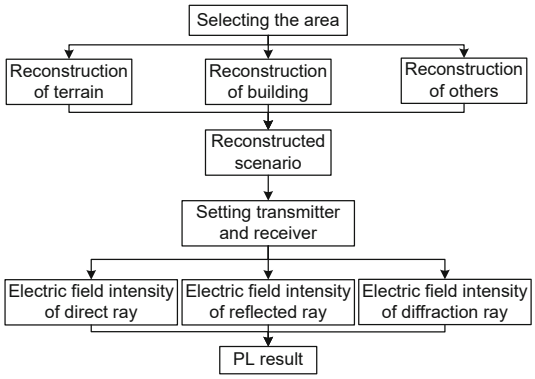

Fig. 3 Flowchart of path loss (PL) prediction

surface. Second, we obtain the length, width, height, latitude, and longitude of the building according to the information in the digital map. To simplify the reconstruction, the bottom surface of a general building can be set as a rectangle of similar size. When encountering a curved building, the surface is decomposed, and then triangles of different sizes are used to piece together a shape similar to the surface. Then, according to the building's height data in the digital map, the building ground is stretched from two-dimension (2D) to 3D. Note that when considering a large terrain with buildings, the triangles will no longer be regular ones in order to connect with all buildings. Fig. 4 shows several typical reconstructed scenarios distinguished by the terrain (i.e., flat, hilly, mountainous, and over water) and different covers.

3.3 Ray-tracing technique

The RT technique has been used for analyzing propagation characteristics since the 1990s, and it performs well for a small specific area and under high-frequency conditions. It describes all the possible propagation paths using a huge number of rays, which can be reflected when interacting with the scatterer surface and diffracted when interacting with the scatterer wedge. After tracking all rays with the forward technique or the reverse technique, propagation parameters, e.g., electric field intensity or amplitude, delay, phase, and angle of each ray, can be obtained. In this study, we focus only on the electric field intensity or amplitude characteristic.

The electric field in the RT process is divided into the direct field, reflection field, and diffraction field. If there is no obstacle between the transmitting point and the receiving point, the electric field

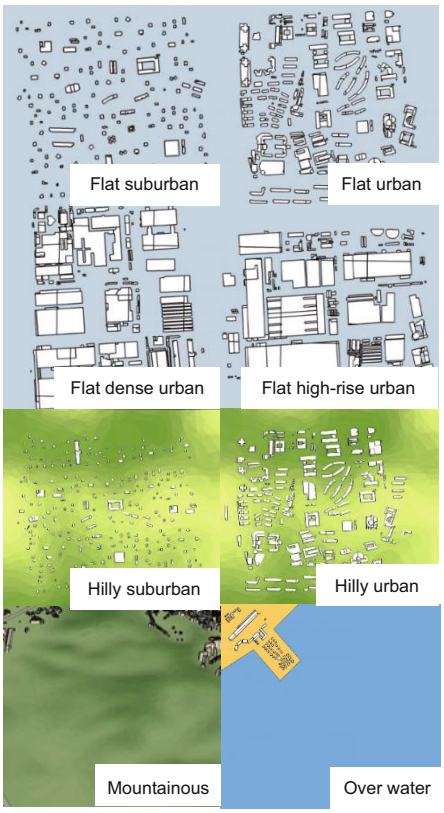

Fig. 4 Reconstructed scenarios

intensity can be calculated by

$$E_{\mathrm{LoS}} = E_0 \cdot \mathrm{e}^{-\mathrm{j}kd}/d, \tag{1}$$

where E_0 is the electric field intensity of 1 m from the transmitter, k is the wave number, and d is the distance between the transmitting point and the receiving point.

When there are obstacles in the propagation process and ray reflection and diffraction are generated, the reflection coefficients of a vertically polarized wave and a horizontally polarized wave should be calculated first, and then the electric field intensity can be calculated as

$$E_{\mathrm{R}} = E_0 R \mathrm{e}^{-\mathrm{j}k(s_1+s_2)}/(s_1+s_2), \tag{2}$$

$$R_{\parallel} = \frac{\varepsilon\cos\theta - \sqrt{\varepsilon\mu - \sin^2\theta}}{\varepsilon\cos\theta + \sqrt{\varepsilon\mu - \sin^2\theta}}, \tag{3}$$

$$R_{\perp} = \frac{\cos\theta - \sqrt{\varepsilon\mu - \sin^2\theta}}{\cos\theta + \sqrt{\varepsilon\mu - \sin^2\theta}}, \tag{4}$$

$$\varepsilon = \varepsilon_{\mathrm{r}} - \mathrm{j}60\lambda\sigma, \tag{5}$$

where θ is the incident angle, ε_{r} is the relative permittivity of the environment, μ is the relative

permeability of the environment, σ is the electrical conductivity of the environment, s_1 is the distance between the transmitting point and the reflected or diffraction point, s_2 is the distance between the receiving point and the reflected or diffraction point, R is the reflection coefficient, and λ is the wave length.

Similarly, the calculation of diffraction electric field intensity can be expressed as

$$E_{\mathrm{D}}=\frac{E_0}{s_1}D\sqrt{\frac{s_1}{s_2(s_1+s_2)}}\mathrm{e}^{-\mathrm{j}k(s_1+s_2)}, \tag{6}$$

where D is the diffraction coefficient. Finally, the electric field intensity vectors that contribute to the receiving points are added together, and the total number of receiving points is

$$E_{\mathrm{total}}=\sum_i E_i, \tag{7}$$

where E_i is the electric field intensity of each receiving point. Note that PL is the ratio of the transmitted power to the received power, so it can be obtained as

$$\mathrm{PL\ (dB)}=20\lg\left(E_{\mathrm{t}}/E_{\mathrm{r}}\right), \tag{8}$$

where E_{t} is the electric field intensity of 1 m range and E_{r} is the electric field vector sum of effective receiving rays.

4 New altitude-dependent mmWave path loss model

4.1 Parametric empirical path loss model

The CI model originates from the free space path loss (FSPL) model, but it considers the shadow fading factor and can adjust the path loss exponent (PLE) by best fitting field data. It has been used for decades in a variety of scenarios and also shown good and robust accuracy over the mmWave frequency band (3GPP, 2016). Like other traditional PL models, the CI model is designed for mobile land communications, and the antenna height factor is not involved. It can be expressed as

$$L^{\mathrm{CI}}\left(f_{\mathrm{c}},d\right)\ [\mathrm{dB}]=32.4+20\lg f_{\mathrm{c}}+10n\lg d+\chi_\sigma, \tag{9}$$

where n is the PLE, χ_σ is a zero-mean Gaussian variable representing the factor of shadow fading, d is the distance in meters, and f_{c} is the carrier frequency in GHz. The 3GPP PL model of the rural macrocell (RMa) scenario is designed for low-altitude (<150 m) communications. In the LoS case, if 10 m $\le d_{\mathrm{2D}} \le d_{\mathrm{BP}}$, it can be expressed as

$$\begin{aligned}L^{\mathrm{3GPP}}_{\mathrm{RMa\text{-}LoS}}\ [\mathrm{dB}]&=20\lg\left(40\pi d f_{\mathrm{c}}/3\right)+0.002(\lg h)d\\&+\min(0.03h^{1.72},10)\lg d-\min(0.044h^{1.72},14.77);\end{aligned} \tag{10}$$

if $d_{\mathrm{BP}} < d_{\mathrm{2D}} \le 10$ km, it can be expressed as

$$\begin{aligned}L^{\mathrm{3GPP}}_{\mathrm{RMa\text{-}LoS}}\ [\mathrm{dB}]&=20\lg\left(40\pi d_{\mathrm{BP}} f_{\mathrm{c}}/3\right)\\&+\min(0.03h^{1.72},10)\lg d_{\mathrm{BP}}+40\lg\left(d/d_{\mathrm{BP}}\right)\\&-\min(0.044h^{1.72},14.77)+0.002(\lg h)d_{\mathrm{BP}}.\end{aligned} \tag{11}$$

In the NLoS case, if 10 m $\le d_{\mathrm{2D}} \le 5$ km, it can be expressed as

$$L^{\mathrm{3GPP}}_{\mathrm{RMa\text{-}NLoS}}\ [\mathrm{dB}]=\max(L^{\mathrm{3GPP}}_{\mathrm{RMa\text{-}LoS}},L_2), \tag{12}$$

$$\begin{aligned}L_2\ [\mathrm{dB}]&=20\lg f_{\mathrm{c}}-7.1\lg W+7.5\lg h\\&-\left(24.37-3.7(h/h_{\mathrm{BS}})^2\right)\lg h_{\mathrm{BS}}\\&+(43.42-3.1\lg h_{\mathrm{BS}})(\lg d-3)\\&-\left(3.2(\lg(11.75h_{\mathrm{UT}}))^2-4.97\right)+161.04,\end{aligned} \tag{13}$$

where h is the average building height, W is the average width of the street, d_{BP} is the 2D breakpoint distance in meters, d_{2D} is the 2D distance between the transmitter (TX) and the receiver (RX), h_{BS} is the height of the base station, and h_{UT} is the height of the user terminal.

Because a UAV's height varies greatly in A2G scenarios, this factor thus has great range and physical significance as other parameters do. In this study, the proposed PL model remains physically grounded to FSPL at a close-in distance but also adds the PLE dependence on UAV heights. It highlights the importance of PLE and encapsulates a fundamental physical basis of frequency dependence due to Friis' equation as

$$\begin{aligned}L\left(f_{\mathrm{c}},d,h_{\mathrm{UAV}}\right)\ [\mathrm{dB}]&=32.4+20\lg f_{\mathrm{c}}\\&+10\left(A\cdot(h_{\mathrm{UAV}})^B\right)\lg d+\chi_\sigma,\end{aligned} \tag{14}$$

where A and B are environment-dependent parameters and may vary greatly in different scenarios. Considering that the prediction results have certain fluctuations due to different scenes and shadow fading, we use a zero-mean Gaussian variable χ_σ to represent ups and downs. It should be mentioned that our proposed PL model is empirical, and that proper parameters for given environments are critical to obtain the

accurate PL. Moreover, this model is more general and suitable for the UAV-to-ground communications by taking the UAV height into consideration, and the fitting data could be from either field measurements or analytical results. It should be mentioned that atmospheric factors are also very important for the high-altitude scenarios, but they are not considered in this study for simplicity.

4.2 Simulation schedule and scenarios

Because measurement campaigns for A2G mmWave channels are difficult and costly, we conducted many RT simulations and obtained voluminous PL data for analysis. In the simulations, the typical communication environment in Fig. 1 was considered. The ground station was fixed as a TX and the UAV as an RX at different heights. The simulation schedule is shown in Fig. 5, where the UAV height ranged from 5 to 1000 m (in a step of 50 m from 50 to 1000 m, plus the first layer at 5 m, i.e., totally 21 layers). For each layer, 4000 randomly distributed points were selected as RXs and the propagation channels were divided into LoS and NLoS cases. Note that in the simulations, we found that the PL values of reflection and diffraction paths varied greatly. Thus, we further divided the NLoS cases into two types, i.e., reflection and diffraction, which created significant advantages in fitting the data. In Fig. 5, we calculated the PL values based on the RT technique and described the propagation conditions as LoS, reflection, and diffraction with different colors.

4.3 Data fitting and analyzing

In this study, the A2G scenarios are classified into four terrain types with different covers. For each scenario, we repeat the simulations to obtain enough data with different UAV heights. As an example, the raw PL data from the high-rise urban scenario with four heights are given in Fig. 6. The fitted curves using the least squares (LS) fit are also given. As we can see, the raw data are concentrated in three groups, which is the basic reason that three cases, i.e., the LoS, reflection, and diffraction, are considered in our proposed model.

To demonstrate the impact of the height of a UAV on the PL, the fitting curves in the high-rise urban scenario with different heights of a UAV are

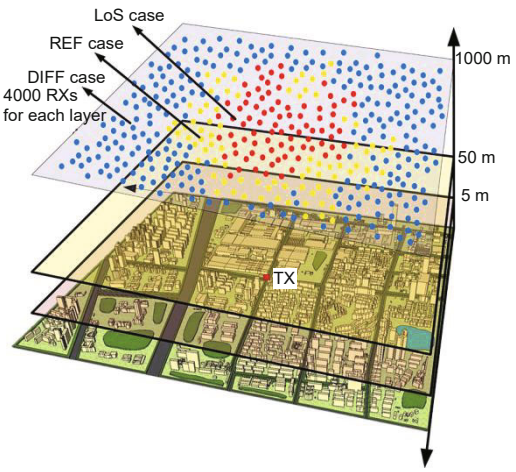

Fig. 5 Simulation schedule (References to color refer to the online version of this figure)

compared in Fig. 7. The figure clearly shows that the LoS PL curves are almost the same as those of the FSPL model, because obstacles have no effect on the PL in the LoS case. The fitting curves at different heights of the UAV in the NLoS cases are significantly different, which is not considered in previous PL models. As we can see, both the reflection and diffraction PLEs decrease as the UAV height increases, because the impact of obstacles decreases. Specifically, the measurement results of the RMa NLoS scenario in the 3GPP model also show that the PL decreases when increasing the antenna height of the BS, which is consistent with our research result (3GPP, 2016; MacCartney and Rappaport, 2017a, 2017b). However, it should be noted that the PL in the 3GPP RMa scenario is suitable only for low-altitude ($<$150 m) communications. Considering that a UAV's flight altitude is generally below 1 km, the height range of 5 to 1000 m of a UAV is considered in this study. However, it should be noted that the above PL prediction method is suitable for higher altitudes.

By fitting the data under different scenarios, we obtain PLEs with different heights of a UAV and calculate parameters A and B. Finally, the best fit parameters for our proposed PL model under different scenarios are summarized in Table 1. In the LoS case, the PL model is not very height-dependent, and parameter B is zero. In the NLoS case, although the values of parameter B are close to zero, the trend of PL changes with height in most scenarios. Because parameter B is the index of an exponential function, a small change would result in a significantly

different PL. For mountainous and over water scenarios, the path is always LoS and thus the NLoS cases are not considered. The raw data of the LoS case under different scenarios are different, but the fitted PLEs are very close with different variance as shown in Table 1. The standard deviation (STD) of

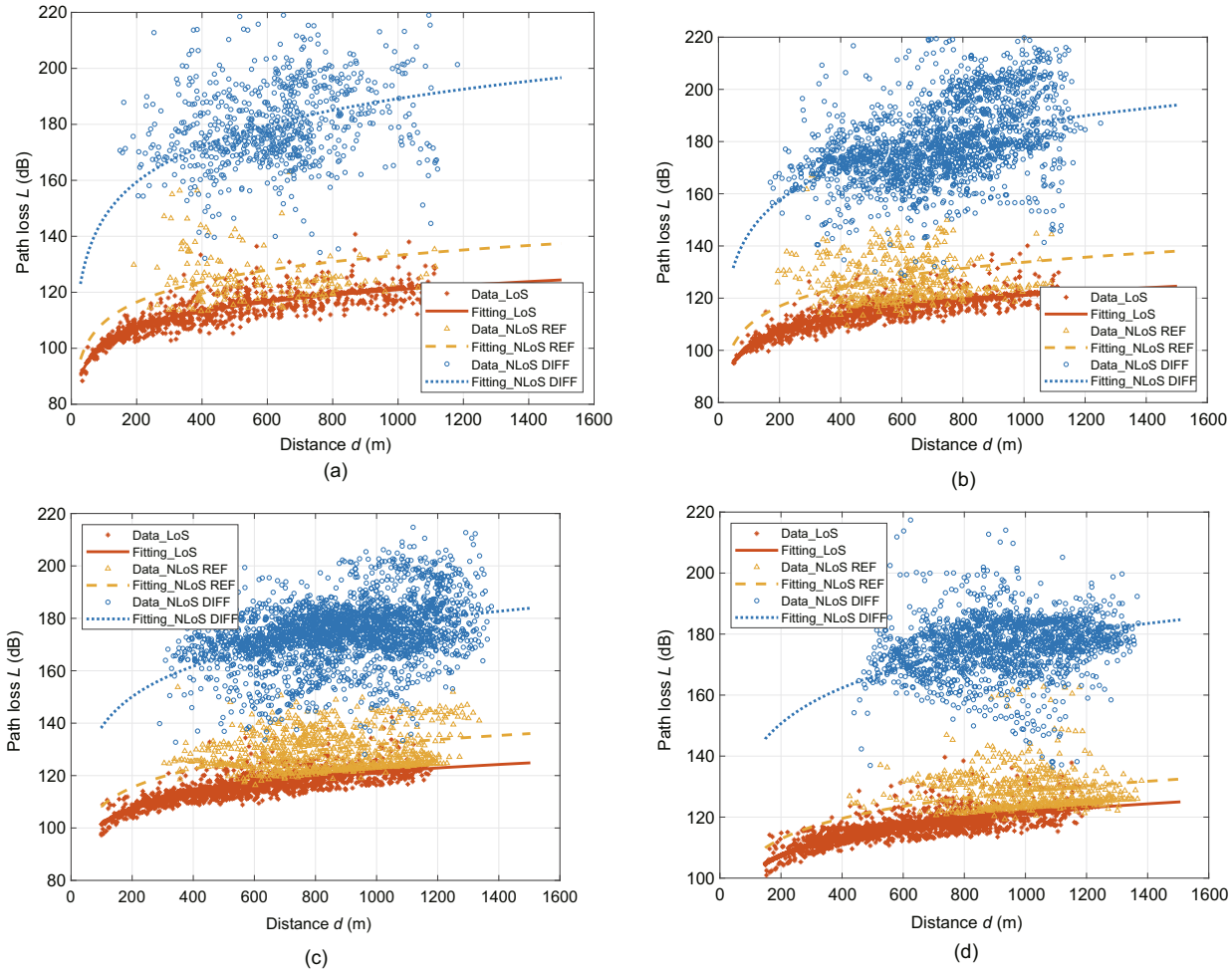

Fig. 6 Data fitting under the high-rise urban scenario with the UAV heights of 30 m (a), 50 m (b), 100 m (c), and 150 m (d)

Table 1 Model parameters for different scenarios

Terrain	Scenario	A			B			σ (dB)		
		LoS	REF	DIFF	LoS	REF	DIFF	LoS	REF	DIFF
Flat	Suburban	2.000	2.406	3.649	0	−0.011 55	−0.047 34	2.24	3.13	6.49
	Urban	2.000	2.999	4.146	0	−0.069 58	−0.017 30	1.44	3.60	6.84
	Dense urban	2.000	2.772	5.619	0	−0.047 24	−0.074 43	1.91	3.53	6.65
	High-rise urban	2.000	2.611	4.921	0	−0.0269	−0.045 86	2.18	3.72	6.18
Hilly	Suburban	2.000	3.474	5.236	0	−0.068 46	−0.059 21	2.74	4.01	6.05
	Urban	2.000	3.052	4.203	0	−0.029 61	−0.018 91	2.32	4.32	6.90
Mountainous	Forest	2.000	–	–	0	–	–	3.44	–	–
	Vegetation	2.000	–	–	0	–	–	2.88	–	–
Over water	Fresh water	2.000	–	–	0	–	–	2.08	–	–
	Sea water	2.000	–	–	0	–	–	2.71	–	–

LoS: line-of-sight; REF: reflection; DIFF: diffraction

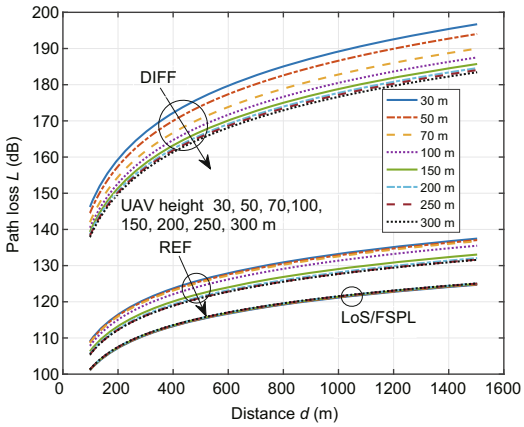

Fig. 7 Fitting curves with different UAV heights under the high-rise urban scenario (References to color refer to the online version of this figure)

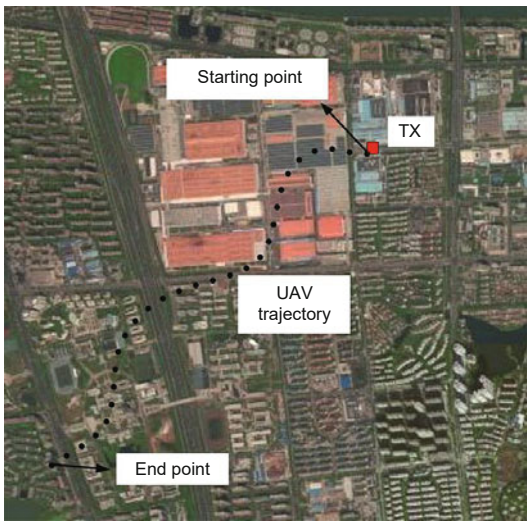

Fig. 8 Satellite view of the high-rise urban scenario

fluctuations in dB is also shown in Table 1. Note that the STD of our proposed model is smaller than those of other models. For example, the STD of the 3GPP RMa PL model is 8 in the NLoS case.

5 Comparison and validation

In this section, we evaluate the effectiveness and performance of the proposed mmWave PL model. The predicted PL is compared with the PLs calculated by other PL models, i.e., the 3GPP PL model of the RMa scenario, the CI model, and the RT method. To verify the proposed PL model, we generate RT data using commercial ray-tracing software Remcom (https://www.remcom.com/wireless-insite-em-propagation-software), which has been approved as a reliable wave propagation calculation tool (Mededović et al., 2012). The satellite view of an area in Nanjing, China is given in Fig. 8. The studied area is a typical high-rise urban scenario. There are 2664 buildings with heights from 5 to 195 m, and most of them are about 55 m. The dimension of the terrain is 2800 m×2800 m, meaning that there are about 340 buildings per square kilometer. The vehicle at the height of 2 m is in the upper right corner, and the UAV carrying the receiver flies along the trajectory shown in black dotted lines at the heights of 50 and 300 m, respectively. The total trajectory is about 1660 m and the UAV position is sampled every 5 m, with a total of 332 sampling points. In the simulation, only six orders of reflection and one order of diffraction are considered, and the remaining parameters are given in Table 2.

Table 2 Simulation parameters

Parameter	Value
Frequency	28 GHz
Bandwidth	500 MHz
Transmitting power	20 dBm
3GPP antenna type	Omnidirectional
UAV height	50, 300 m
Vehicle height	2 m

Figs. 9a and 9b present the prediction results of different PL models for UAV flight along the trajectory at the heights of 50 and 300 m, respectively. For comparison, the calculation results by the RT method are also given in Fig. 9. It is worth mentioning that the 3GPP model is designed for low-altitude (<150 m) communications. When the UAV height is 50 m, the three PL models have similar results for the LoS case. For the NLoS case, the 3GPP model may consider more of the reflection, but the CI model averages the effects of reflection and diffraction (Fig. 9a). It is reasonable to achieve better performance because we consider reflection and diffraction. When the UAV is at 300 m, the 3GPP model is no longer suitable and the NLoS PL is almost the same as in the LoS case. The CI model does not have a height limitation, but it does not reflect the impact of UAV height. For the high-altitude case, PL values in the NLoS case would vary significantly. From Fig. 9, it can be seen that the proposed method has better performance than the other two models, because it considers the effects of the environment, UAV height, and propagation conditions.

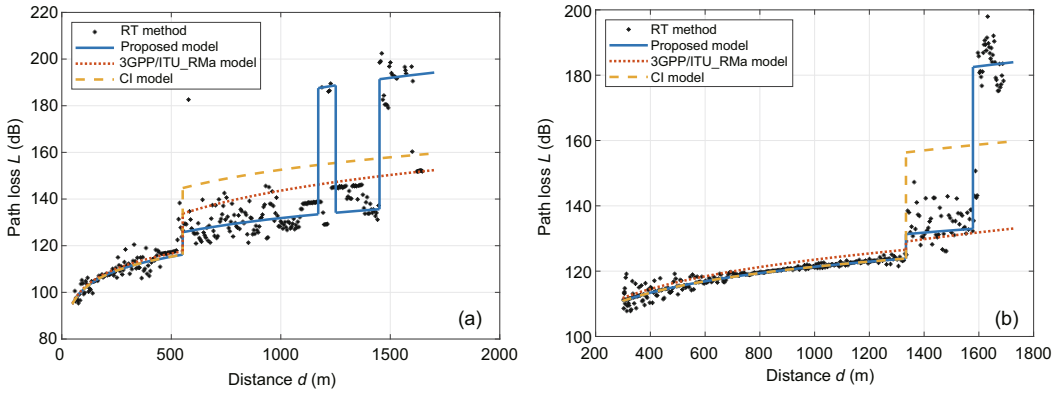

Fig. 9 Comparison of different PL models with the UAV heights of 50 m (a) and 300 m (b)

6 Conclusions

In this paper, we have proposed a general empirical PL model for A2G mmWave communications considering the effects of environment, frequency, distance, and UAV height. A deterministic PL calculation algorithm based on the digital map and RT technique has been developed. The reconstruction process of the 3D scattering scenario has also been presented to reduce the calculation complexity. By fitting and analyzing numerous PL data, we have presented the optimized model parameters with respect to the altitude for different scenarios. Taking the high-rise urban scenario as an example, the simulation results showed that our proposed model better matches the RT method than other typical PL models for both low- and high-altitude cases. Moreover, the new model is general and adaptable to other A2G conditions by adjusting the model parameters according to the channel data.

Contributors

Qiuming ZHU and Xiaomin CHEN designed the research. Mengtian YAO and Fei BAI ran the simulations and processed the data. Qiuming ZHU and Mengtian YAO drafted the manuscript. Xiaomin CHEN and Weizhi ZHONG helped organize the manuscript. Boyu HUA, Xiaomin CHEN, and Xijuan YE helped revise the paper. Qiuming ZHU, Mengtian YAO, Fei BAI, and Xiaomin CHEN finalized the paper.

Compliance with ethics guidelines

Qiuming ZHU, Mengtian YAO, Fei BAI, Xiaomin CHEN, Weizhi ZHONG, Boyu HUA, and Xijuan YE declare that they have no conflict of interest.

References

3GPP, 2016. Technical Specification Group Radio Access Network; Channel Model for Frequency Spectrum above 6 GHz (Release 14). TR 38.900 V14.2.0. 3rd Generation Partnership Project (3GPP).

Al-Hourani A, Gomez K, 2018. Modeling cellular-to-UAV path-loss for suburban environments. *IEEE Wirel Commun Lett*, 7(1):82-85. https://doi.org/10.1109/LWC.2017.2755643

Bhuvaneshwari A, Hemalatha R, Satyasavithri T, 2015. Path loss prediction analysis by ray tracing approach for NLOS indoor propagation. Proc Int Conf on Signal Processing and Communication Engineering Systems, p.486-491. https://doi.org/10.1109/SPACES.2015.7058202

Cai XS, Wang NX, Rodríguez-Piñeiro J, et al., 2019. Low altitude air-to-ground channel characterization in LTE network. Proc 13th European Conf on Antennas and Propagation, p.1-5.

Chen XM, Hu XJ, Zhu QM, et al., 2018. Channel modeling and performance analysis for UAV relay systems. *China Commun*, 15(12):89-97. https://doi.org/10.12676/j.cc.2018.12.007

Cheng LL, Zhu QM, Wang CX, et al., 2020. Modeling and simulation for UAV air-to-ground mmWave channels. Proc 14th European Conf on Antennas and Propagation, p.1-5. https://doi.org/10.23919/EuCAP48036.2020.9136077

Cui ZZ, Briso-Rodríguez C, Guan K, et al., 2019. Measurement-based modeling and analysis of UAV air-ground channels at 1 and 4 GHz. *IEEE Antenn Wirel Propag Lett*, 18(9):1804-1808. https://doi.org/10.1109/LAWP.2019.2930547

Dutta S, Hsieh F, Vook FW, 2019. HAPS based communication using mmWave bands. Proc IEEE Int Conf on Communications, p.1-6. https://doi.org/10.1109/ICC.2019.8761640

Fan W, Carton I, Nielsen JØ, et al., 2016. Measured wideband characteristics of indoor channels at centimetric and millimetric bands. *EURASIP J Wirel Commun Netw*, 2016(1):58. https://doi.org/10.1186/s13638-016-0548-x

Hur S, Baek S, Kim B, et al., 2016. Proposal on millimeter-wave channel modeling for 5G cellular system. *IEEE J Sel Top Signal Process*, 10(3):454-469. https://doi.org/10.1109/JSTSP.2016.2527364

ITU, 2017. Terrain Cover Types. International Telecommunication Union.

Khawaja W, Guvenc I, Matolak DW, et al., 2019. A survey of air-to-ground propagation channel modeling for unmanned aerial vehicles. *IEEE Commun Surv Tut*, 21(3):2361-2391. https://doi.org/10.1109/COMST.2019.2915069

Li JF, Zhang XF, Cao RZ, et al., 2013. Reduced-dimension MUSIC for angle and array gain-phase error estimation in bistatic MIMO radar. *IEEE Commun Lett*, 17(3):443-446. https://doi.org/10.1109/LCOMM.2013.012313.122113

MacCartney GR, Rappaport TS, 2017a. Rural macrocell path loss models for millimeter wave wireless communications. *IEEE J Sel Areas Commun*, 35(7):1663-1677. https://doi.org/10.1109/JSAC.2017.2699359

MacCartney GR, Rappaport TS, 2017b. Study on 3GPP rural macrocell path loss models for millimeter wave wireless communications. Proc IEEE Int Conf on Communications, p.1-7. https://doi.org/10.1109/ICC.2017.7996793

MacCartney GR, Rappaport TS, Sun S, et al., 2015. Indoor office wideband millimeter-wave propagation measurements and channel models at 28 and 73 GHz for ultra-dense 5G wireless networks. *IEEE Access*, 3:2388-2424. https://doi.org/10.1109/ACCESS.2015.2486778

Mani F, Vitucci EM, Barbiroli M, et al., 2018. 26GHz ray-tracing pathloss prediction in outdoor scenario in presence of vegetation. Proc 12th European Conf on Antennas and Propagation, p.1-5. https://doi.org/10.1049/cp.2018.0384

Mededović P, Veletić M, Blagojević Z, 2012. Wireless in-site software verification via analysis and comparison of simulation and measurement results. Proc 35th Int Convention MIPRO, p.776-781.

Rappaport TS, MacCartney GR, Samimi MK, et al., 2015. Wideband millimeter-wave propagation measurements and channel models for future wireless communication system design. *IEEE Trans Commun*, 63(9):3029-3056. https://doi.org/10.1109/TCOMM.2015.2434384

Rappaport TS, Sun S, Shafi M, 2017a. Investigation and comparison of 3GPP and NYUSIM channel models for 5G wireless communications. Proc IEEE 86th Vehicular Technology Conf, p.1-5. https://doi.org/10.1109/VTCFall.2017.8287877

Rappaport TS, Xing YC, MacCartney GR, et al., 2017b. Overview of millimeter wave communications for fifth-generation (5G) wireless networks—with a focus on propagation models. *IEEE Trans Antenn Propag*, 65(12):6213-6230. https://doi.org/10.1109/TAP.2017.2734243

Samimi MK, Rappaport TS, MacCartney GR, 2015. Probabilistic omnidirectional path loss models for millimeter-wave outdoor communications. *IEEE Wirel Commun Lett*, 4(4):357-360. https://doi.org/10.1109/LWC.2015.2417559

Shi Y, Enami R, Wensowitch J, et al., 2018. Measurement-based characterization of LOS and NLOS drone-to-ground channels. Proc IEEE Wireless Communications and Networking Conf, p.1-6. https://doi.org/10.1109/WCNC.2018.8377104

Sun S, Rappaport TS, Thomas TA, et al., 2016. Investigation of prediction accuracy, sensitivity, and parameter stability of large-scale propagation path loss models for 5G wireless communications. *IEEE Trans Veh Technol*, 65(5):2843-2860. https://doi.org/10.1109/TVT.2016.2543139

Wang CX, Bian J, Sun J, et al., 2018. A survey of 5G channel measurements and models. *IEEE Commun Surv Tut*, 20(4):3142-3168. https://doi.org/10.1109/COMST.2018.2862141

Wang XY, Gursoy MC, 2019. Coverage analysis for energy-harvesting UAV-assisted mmWave cellular networks. *IEEE J Sel Areas Commun*, 37(12):2832-2850. https://doi.org/10.1109/JSAC.2019.2947929

Wu YY, Gao ZB, Chen CB, et al., 2015. Ray tracing based wireless channel modeling over the sea surface near Diaoyu Islands. Proc 1st Int Conf on Computational Intelligence Theory, Systems and Applications, p.124-128. https://doi.org/10.1109/CCITSA.2015.35

Yang GS, Zhang Y, He ZW, et al., 2019. Machine-learning-based prediction methods for path loss and delay spread in air-to-ground millimetre-wave channels. *IET Micro Antenn Propag*, 13(8):1113-1121. https://doi.org/10.1049/iet-map.2018.6187

You XH, Wang CX, Huang J, et al., 2021. Towards 6G wireless communication networks: vision, enabling technologies, and new paradigm shifts. *Sci China Inform Sci*, 64(1):110301. https://doi.org/10.1007/s11432-020-2955-6

Zhang JH, Shafi M, Molisch A, et al., 2018. Channel models and measurements for 5G. *IEEE Commun Mag*, 56(12):12-13. https://doi.org/10.1109/MCOM.2018.8570033

Zhao XW, Du F, Geng SY, et al., 2020. Playback of 5G and beyond measured MIMO channels by an ANN-based modeling and simulation framework. *IEEE J Sel Area Commun*, 38(9):1945-1954. https://doi.org/10.1109/JSAC.2020.3000827

Zhong WZ, Xu L, Zhu QM, et al., 2019a. MmWave beamforming for UAV communications with unstable beam pointing. *China Commun*, 16(1):37-46.

Zhong WZ, Xu L, Zhu QM, et al., 2019b. A novel beam design method for mmWave multi-antenna arrays with mutual coupling reduction. *China Commun*, 16(10):37-44. https://doi.org/10.23919/JCC.2019.10.002

Zhu QM, Li H, Fu Y, et al., 2018. A novel 3D non-stationary wireless MIMO channel simulator and hardware emulator. *IEEE Trans Commun*, 66(9):3865-3878. https://doi.org/10.1109/TCOMM.2018.2824817

Zhu QM, Wang YW, Jiang KL, et al., 2019. 3D non-stationary geometry-based multi-input multi-output channel model for UAV-ground communication systems. *IET Microw Antenn Propag*, 13(8):1104-1112. https://doi.org/10.1049/iet-map.2018.6129

Zhu QM, Jiang S, Wang CX, et al., 2020. Effects of digital map on the RT-based channel model for UAV mmWave communications. Proc Int Wireless Communications and Mobile Computing, p.1648-1653. https://doi.org/10.1109/IWCMC48107.2020.9148461